BIOCHEMISTRY
including biophysical chemistry & molecular biology
Article

Biochemistry **2009,** *48,* 11185–11195 11185
DOI: 10.1021/bi900998v

Interaction of the Tim44 C-Terminal Domain with Negatively Charged Phospholipids[†]

Milit Marom,[‡] Roman Safonov,[‡] Shay Amram,[§] Yoav Avneon,[§] Esther Nachliel, Menachem Gutman, Keren Zohary, Abdussalam Azem,* and Yossi Tsfadia*

Department of Biochemistry, George S. Wise Faculty of Life Sciences, Tel Aviv University, Tel Aviv 69978, Israel
[‡]*These authors contributed equally to this work.* [§]*These authors contributed equally to this work.*

Received June 14, 2009; Revised Manuscript Received October 26, 2009

ABSTRACT: The translocation of proteins from the cytosol into the mitochondrial matrix is mediated by the coordinated action of the TOM complex in the outer membrane, as well as the TIM23 complex and its associated protein import motor in the inner membrane. The focus of this work is the peripheral inner membrane protein Tim44. Tim44 is a vital component of the mitochondrial protein translocation motor that anchors components of the motor to the TIM23 complex. For this purpose, Tim44 associates with the import channel by direct interaction with the Tim23 protein. Additionally, it was shown in vitro that Tim44 associates with acidic model membranes, in particular those containing cardiolipin. The latter interaction was shown to be mediated by the carboxy-terminal domain of Tim44 [Weiss, C., et al. (1999) *Proc. Natl. Acad. Sci. U.S.A. 96*, 8890−8894]. The aim of this study was to determine the precise recognition site for negative lipids in the C-terminal domain of Tim44. In particular, we wanted to examine the recently suggested hypothesis that acidic phospholipids associate with Tim44 via a hydrophobic cavity that is observed in the high-resolution structure of the C-terminal domain of the protein [Josyula, R., et al. (2006) *J. Mol. Biol. 359*, 798−804]. Molecular dynamics simulations suggest that (i) the hydrophobic tail of lipids may interact with Tim44 via the latter's hydrophobic cavity and (ii) a region, located in the N-terminal α-helix of the C-terminal domain (helices A1 and A2), may serve as a membrane attachment site. To validate this assumption, N-terminal truncations of yeast Tim44 were examined for their ability to bind cardiolipin-containing phospholipid vesicles. The results indicate that removal of the N-terminal α-helix (helix A1) abolishes the capacity of Tim44 to associate with cardiolipin-containing liposomes. We suggest that helices A1 and A2, in Tim44, jointly promote the association of the protein with acidic phospholipids.

The import of nuclear-encoded proteins into the mitochondria is a multistep process that is mediated by the coordinated action of translocation machineries localized in both the outer and inner mitochondrial membranes. In the outer membrane, the multimeric TOM[1] complex serves as both a receptor for recognition of mitochondrial precursor proteins and a main portal of entry for proteins into mitochondria (*1*−*3*). On their way to the matrix, proteins that contain cleavable amino-terminal targeting signals (MTS) are transferred from the TOM complex to the TIM23 preprotein translocase. The core of this complex is composed of two multispanning, integral, inner-membrane proteins Tim23 and Tim17. The former forms a channel that allows proteins to be integrated into or to cross the inner membrane. A third protein, Tim50, seems to serve as a sorting receptor in the mitochondrial intermembrane space and regulates the pore formed by Tim23 (*4*, *5*). A precursor protein in transit across the Tim23 channel requires additional help to be imported completely into the mitochondrial matrix. This step is catalyzed by a translocation motor that is formed by the ATP-hydrolyzing 70 kDa heat-shock protein (mtHsp70), its J-domain-containing cochaperones Tim14 (Pam18) and Tim16 (Pam16), and the nucleotide exchange factor, Mge1. A further central component, Tim44 is suggested to associate transiently with the TIM23 complex and to recruit mtHsp70 to the import channel in a nucleotide-dependent manner. Mge1 and the Tim14 (Pam18)−Tim16 (Pam16) complex most likely modulate the function of the motor (*6*). Two proteins, Pam17 and Tim21 play antagonistic roles in regulating the import channel (*7*−*10*).

In a previous study, we investigated the domain structure of purified Tim44 and its interaction with model membranes in vitro (*11*). Using limited proteolysis, we found that Tim44 is composed of an N-terminal domain that is rapidly degraded by proteases and a C-terminal domain that is very stable when treated with proteases. A study of the interaction of purified Tim44 with model membranes demonstrated that the protein associates with monolayers and liposomes composed of acidic phospholipids. Finally, we found that the C-terminus of Tim44, similar to the full-length protein, interacts with liposomes that contain the phospholipid cardiolipin but not with liposomes that are composed of phosphatidylcholine alone (*11*). Cardiolipin is the major acidic phospholipid of the mitochondrial inner

[†]This work was supported by the German-Israeli Foundation for Scientific Research and Development (GIF) (Grant 753/181) and the German-Israeli Project Cooperation (DIP) (Grant F5.1).

*To whom correspondence should be addressed. A.A.: Tel Aviv University, Tel Aviv 69778, Israel; phone, +97236409007; fax, +97236406834; e-mail, azema@tauex.tau.ac.il. Y.T.: Tel Aviv University, Tel Aviv, 69978, Israel; phone, +97236405766; fax, +97236405766; e-mail, yossit@tauex.tau.ac.il.

[1]Abbreviations: LJ, Lennard-Jones; MD, molecular dynamics; PDB, Protein Data Bank; PLM, palmitate anion; rmsd, root-mean-square deviation; SPC, simple point charge; VdW, van der Waals; VMD, visual molecular dynamics; mtHsp70, 70 kDa mitochondrial heat-shock protein; Tim, translocase of the inner mitochondrial membrane; Tom, translocase of the outer mitochondrial membrane; Pam, presequence translocase-associated motor; CL, cardiolipin; PC, phosphatidylcholine.

Published on Web 10/28/2009

Table 1: Primers Used for Site-Directed Mutagenesis

introduced mutation	primer name	primer sequence
V306A	V306A-1	5′ CCC GAG ATT CTC GAA GCG TAT GCG AAA GGC GAT GTC 3′
	V306A-2	5′ GAC ATC GCC TTT CGC ATA CGC TTC GAG AAT CTC GGG 3′
G388A	G388A-1	5′ GGC GAG ATT GCG GCT GCT GAC GAA GCT AAT ATC 3′
	G388A-2	5′ GAT ATT AGC TTC GTC AGC AGC CGC AAT CTC GCC 3′
Y398A	Y398A-1	5′ C TTG ATG AGC TCT GCT GCC ATG GTT TTC ACC AGA GAC CC 3′
	Y398A-2	5′ GG GTC TCT GGT GAA AAC CAT GGC AGC AGA GCT CAT CAA G 3′
F422A	F422A-1	5′ GGG TGG AAG ATC TTG GAG GCT GTG CGC GGG GG 3′
	F422A-2	5′ CC CCC GCG CAC AGC CTC CAA GAT CTT CCA CCC 3′

Table 2: Primers Used for Cloning Various Constructs in Bacterial Expression Vectors

Construct Name	Primer Name	Primer Sequence
Tim44	Tim44-Nt	5′ TAA GGA TCC CAA GGT GGA AAC CCT CGA 3′
	Tim44-Ct	5′ TAA GCG GCC GCT CAG GTG AAT TGT CTA GA 3′
Tim44 C-ter	Tim44-Cter-Nt	5′ GGA TCC ACA AAT ATC GAG TCT AAA GAA 3′
	Tim44-Cter-Ct	5′ TAA GCG GCC GCT CAG GTG AAT TGT CTA GA 3′
Tim44−235	Tim44−235-Nt	5′ GGA TCC ATA CAA TCT TTA AAG AAC 3′
	Tim44-Ct	5′ TAA GCG GCC GCT CAG GTG AAT TGT CTA GA 3′
Tim44−244	Tim44−244-Nt	5′ TAA GGA TCC GAT GAA AGT GAA AAC CCC TTA 3′
	Tim44-Ct	5′ TAA GCG GCC GCT CAG GTG AAT TGT CTA GA 3′
Tim44−263	Tim44−263-Nt	5′ TAA GGA TCC GGT TTC TTT GCA GAA ACA GAA 3′
	Tim44-Ct	5′ TAA GCG GCC GCT CAG GTG AAT TGT CTA GA 3′
A1-A2-Mge1	Tim44−211-Nt	5′ GGA TCC AAT ATC GAG TCT AAA GAA TCG 3′
	Mge1-Tim44-Ct	5′ GGA TTC TTC ACT TTT GGC TTC ATC AGA ATA GGA TTC TGT TTC TGC AAA GAA ACC GCC 3′
	Tim44-Mge1-Nt	5′ GGC GGT TTC TTT GCA GAA ACA GAA TCC TAT TCT GAT GAA GCC AAA AGT GAA GAA TCC 3′
	Mge1-Ct	5′ GCG GCC GCT TAG TTC TCT TCG CCC TTA AC 3′

membrane and is associated with many functions in the cell (*12*−*18*). As such, the presence of cardiolipin was shown to be required for integration of the functional motor-free form of the TIM23 complex into proteoliposomes (*17*, *19*) and to associate with Tim12, a member of the small Tim chaperone family (*20*). Hence, we believe that the preference of Tim44 for cardiolipin represents an important finding with wider significance.

The region or specific amino acids of Tim44 that mediate its interaction with acidic membranes are largely unknown. Additionally, the physical nature of the forces that lead to the attachment of Tim44 to the membrane is obscure. Recently, two crystal structures of the C-terminal domain of Tim44 have been published: the human Tim44 and the yeast Tim44 (PDB entries 2CW9 and 2FXT, respectively) (*21*, *22*). The overall topologies of the yeast and human Tim44 look similar when they are superimposed on each other. The structure of the C-terminal domain of Tim44 consists of six α-helices and four *β*-strands. In the crystal structure, a large hydrophobic pocket was identified on the surface of the protein (15 Å × 10 Å × 10 Å). The hydrophobic pocket was marked by the authors (*22*) as the site that binds phospholipid acyl groups, possibly contributing to the association of Tim44 with acidic model membranes. This identification poses some orientation difficulty, as the acyl residues of the membrane are not well exposed to the surface.

The aim of this study was to determine regions of the Tim44 structure that mediate its interaction with model membranes. Through MD modeling simulations and in vitro liposome binding assays, we show that the interaction of Tim44 with acidic phospholipids is mediated by the cooperation of two α-helices (A1 and A2) that are located at the amino terminus of the C-terminal domain.

EXPERIMENTAL PROCEDURES

Site-Directed Mutagenesis. Point mutations were created by the QuikChange site-directed mutagenesis kit (Stratagene catalog no. 200519). Primers used for mutagenesis (Table 1) were designed according to the manufacturer's guidelines, and Tim44 that was cloned into a modified pET-21d(+) plasmid served as a template (*23*). Following temperature cycling, the product was treated with DpnI endonuclease to digest the methylated parental DNA template. The DNA was then transformed into XL1-Blue *Escherichia coli* competent cells and plated on LB-Amp agar plates. Plasmids were isolated from colonies and sequenced to confirm the presence of the introduced mutation. The mutated plasmid was transformed into BL21 *E. coli* competent cells for expression.

Purification of Recombinant Full-Length Tim44 and Its Various Constructs. Purification of the Tim44 C-terminal domain, Tim44−235, Tim44−244, Tim44−263, and the mutants (V306S and G388A) was conducted essentially as described previously for purification of full-length wild-type Tim44 (*23*). Sodium dodecyl sulfate−polyacrylamide gel electrophoresis (SDS−PAGE) of the various purified constructs is presented in Figure S1 (Supporting Information). Primers used for cloning the various constructs are listed in Table 2.

Construction of a Fusion Protein from Helices A1 and A2 and Mge1. The fusion between helices A1 and A2 of Tim44 (amino acids 211−270) and Mge1 (lacking 43 amino acids, which constitute the N-terminal mitochondrial targeting signal) was created using overlapping polymerase chain reaction (PCR). The final construct contained Mge1 fused to helices A1 and A2, at its amino terminus. Additionally, the construct contained an

octahistidine tag at its amino terminus, with an engineered TEV protease cleavage site between the termini, allowing for removal of the His tag by proteolysis (*23*). The primers used for this purpose are listed in Table 2. The cloning of Mge1 carrying a C-terminal hexahistidine tag has been described previously (*24*).

Purification of the A1-A2-Mge1 Fusion and Mge1. Bacteria were grown for ~3 h at 37 °C in LB medium (6 L) containing either 100 μg/mL ampicillin and 25 μg/mL kanamycin for bacteria expressing Mge1$(His)_6$ or 100 μg/mL ampicillin and 34 μg/mL chloramphenicol for bacteria expressing $(His)_8$-A1-A2-Mge1. When an A_{600} of 0.6 was reached, protein expression was induced with 1 mM isopropyl β-D-1-thiogalactopyranoside for 3 h. Bacteria were collected by centrifugation at 5000 rpm for 10 min and homogenized in 60 mL of lysis buffer containing 50 mM Tris-HCl (pH 7.4), 10% glycerol, 250 mM KCl, 2 mM β-mercaptoethanol, 10 mM $MgCl_2$, 1% Triton X-100, 0.05 mg/mL lysozyme, 45 μg/mL DNase, 2 mM phenylmethanesulfonyl fluoride, and one tablet of complete EDTA-free protease inhibitor mixture (Roche catalog no. 05 056 489 001). After incubation for 15 min on ice, the bacteria were disrupted using a microfluidizer. Insoluble material was removed by centrifugation at 14000 rpm for 30 min at 4 °C. The soluble fraction was loaded onto a Ni-agarose column (20 mL) pre-equilibrated with buffer A [50 mM Tris-HCl (pH 7.4), 10% glycerol, 250 mM KCl, 2 mM β-mercaptoethanol, and 5 mM imidazole]. The column was washed with 3 volumes of buffer A until a stable baseline was reached. The fractions were eluted with a linear gradient (from 0 to 50%, 90 mL) of buffer B (buffer A containing 1 M imidazole). The fractions enriched with the protein were pooled and treated with TEV protease (TEV:protein ratio of 1:40, w/w) overnight at 4 °C in a dialysis bag, against 5 L of buffer A. The protein was then passed over a second Ni-agarose column to remove the TEV protease, which itself contains an uncleavable octahistidine tag, as well as proteins containing uncleaved histidine tags. Fractions enriched with the protein were concentrated. In the final step, the proteins were loaded onto a HiLoad 16/60 Superdex 75 column (total bead volume, 90 mL; Amersham Biosciences) pre-equilibrated with 20 mM Na-HEPES (pH 7.4) and 300 mM NaCl at a flow rate of 1 mL/min. Fractions with the desired protein were concentrated using Vivaspin protein concentrators (Vivascience; molecular weight cutoff of 3000), divided into aliquots, and flash-frozen in liquid N_2. All of the purification procedures were conducted at 4 °C.

In some experiments, we examined the ability of the A1-A2-Mge1 fusion to bind liposomes without removal of the histidine tag. The purification of the proteins was similar to that described in this section, but without the TEV treatment (i.e., the protein was loaded on the gel filtration column directly after the Ni-agarose column).

Preparation of Sucrose-Loaded Liposomes. Sucrose-loaded liposomes were prepared as described previously, with minor modifications (*11*, *25*, *26*). Synthetic dioleoylphosphatidylcholine (PC, Sigma-Aldrich catalog no. P6354), 10 mg, with cardiolipin from bovine heart (CL, Sigma-Aldrich catalog no. C0563) (5:1, w/w) or PC alone was dissolved in 1 mL of chloroform in a round-bottomed flask and dried using rotary evaporation (RE 111 rotavapor and 461 water bath, Buchi). The dry lipid mixture was suspended in 1 mL of buffer A, containing 500 mM sucrose and 10 mM Na-HEPES (pH 7.4), and mixed by vortex. We produced multilamellar vesicles (MLVs) by freezing a flask containing the lipids in liquid nitrogen and subsequently thawing it in a 40 °C water bath. The freeze−thaw cycle was repeated five times. The MLVs were then converted to LUVs by being passed 10 times through two 100 nm polycarbonate membranes. This was conducted using a mini-extruder (Avanti Polar Lipids catalog no. 610023), until homogeneously sized, sucrose-loaded, unilamellar liposomes were obtained. The resulting solution was diluted 5-fold in buffer B, containing 100 mM KCl, 100 mM NaCl, and 10 mM Na-HEPES (pH 7.4). The suspension was centrifuged at 55000 rpm (137000*g*) for 1 h at 22 °C (Sorvall Discovery M120 SE, S120-AT2 rotor). After the supernatant had been removed, the pellet was resuspended in 500 μL of buffer B by incubation for 15 min at room temperature.

Binding of Tim44 to Liposomes. Sucrose-loaded vesicles, composed of either PC or a mixture of PC and CL (5:1), were incubated with 1 μM Tim44 for 1 h in 200 μL of buffer B at 22 °C. Tim44 that bound to the liposomes was separated from unbound Tim44 by centrifugation at 55000 rpm (Sorvall Discovery M120 SE, S100-AT3 rotor) for 1 h at 22 °C. The pelleted fractions were analyzed on a 14% polyacrylamide gel. The gel was stained with Coomassie dye, and the amount of bound Tim44 was determined by optical densitometry (Genesys 10 UV, Thermo Scientific).

MD Simulations. The MD simulations were performed using the GROMACS 3.3.1 package of programs (*27*−*29*) with the GROMOS96 53A6 force field (*30*). The coordinates for the yeast and human Tim44 C-terminal domain (PDB entries 2FXT and 2CW9, respectively), determined by X-ray crystallography at 1.9 Å (*21*, *22*), were downloaded from the Protein Data Bank (*31*). The C-terminus of Tim44 was selected to be in the COO^- form, due to the common state of the carboxyl group at the pH level on the matrix side of the mitochondria (pH ~8.00). However, the N-terminus of the C-domain in vivo is linked to the N-domain (which was not crystallized) through a peptide bond. Thus, we set the N-terminus of the C-domain to be uncharged (NH_2) in silico, to better emulate the native protein and avoid artificial positive charge. In addition to the simulations of the published structure of the yeast Tim44 C-domain, we have also included several simulations using the C-terminal domain that was elongated in silico by 14 amino acids (Lys 220−Arg 233). Elongation was facilitated using Swiss-PDB Viewer (*32*). The 14 residues were added to helix A1 as an extension of the existing α-helix. The palmitate (PLM) anion geometry was taken from the PRODRG server for small molecules (*33*). Its force field (FF) parameters were taken from the carboxylate parameters of the GROMOS96 force field. The protein and the ligand were embedded in a truncated octahedral box containing approximately 20000−30000 water molecules using the SPC water model (*34*) that extended at least 12 Å from the protein.

A total of 11 simulations of the protein with PLM were performed, three with the human Tim44 protein, four with the yeast "short" Tim44, and four with the elongated one (Table 3). Each simulation had a different initial location of the PLM ions and initial velocities. The PLM ions were randomly placed within the water box, but special care was taken to ensure that the initial position of the PLM ions was some distance from the protein's surface.

Prior to the MD simulations, internal constraints were relaxed by energy minimization. Following the minimization, 100 ps equilibration runs were performed under positional restraints of the carbon backbone atoms through a harmonic force constant of 1000 kJ nm^{-2} followed by unrestrained MD simulations. The first 1000 ps of the runs was treated as a further equilibration simulation, and the remainder was saved and used for the analysis. During the MD runs, the LINCS algorithm (*35*) was

Table 3: Yeast and Human Tim44 C-Terminal Domain Simulations with PLM

protein source	Tim44 type[a]	no. of PLMs[b]	simulation time (ns)
human control A	−	0	14
human control B	−	0	14
human control C	−	0	12
human A	−	4	20
human B	−	4	20
human C	−	4	20
S-yeast control A	short	0	20
S-yeast control B	short	0	20
S-yeast control C	short	0	20
S-yeast A	short	4	20
S-yeast B	short	4	20
S-yeast C	short	4	20
S-yeast D	short	4	20
E-control A	elongated	0	20
E-control B	elongated	0	20
E-control C	elongated	0	20
E-yeast A	elongated	4	20
E-yeast B	elongated	4	20
E-yeast C	elongated	4	20
E-yeast D	elongated	4	20

[a]The short type refers to that in the original PDB file downloaded from the Protein Data Bank. Elongation of Tim44 was by 14 residues on the N-terminal side of the C-domain (K220→KVEDFKEKTVVGR→S234). The addition was generated using Swiss-PDB Viewer (*32*). [b]Number of PLMs in the simulation box.

used to constrain the lengths of all bonds; the water molecules were restrained using the SETTLE algorithm (*36*). The time step for the simulations was 2 fs. The simulations were run under NPT conditions, using Berendsen's coupling algorithm for keeping the temperature and the pressure constant (P = 1 bar; τ_P = 0.5 ps; τ_T = 0.1 ps; T = 300 K) (*37*). van der Waals (VdW) forces were treated using a cutoff of 12 Å. Long-range electrostatic potentials (r > 12 Å) were treated using the particle mesh Ewald method (*38*). The coordinates were saved every 2 ps. All protein figures were created using the VMD computer program (*39*)

Spatiotemporal Analysis of Ligand Binding. This analysis traces the residues that were below a certain cutoff distance from the carboxylate moiety of palmitate. The screening scanned all snapshots, and the results are presented in a figure in which the residue is identified on the ordinate and the existence of a contact with carboxylate is marked by a colored dot. Thus, a solid horizontal line implies that certain residues remained in the proximity of the ligand for a given length of time. The analysis was conducted for all simulations with an accumulated simulation time of 160 ns.

RESULTS

Binding of the C-Terminal Domain of Tim44 to Sucrose-Loaded Liposomes. The suggestion that Tim44 associates with acidic phospholipids via its C-terminal domain was based upon indirect evidence, namely, that the C-terminal domain was protected from trypsin digestion when incubated with acidic phospholipids (*11*). Additionally, the Tim44 in that report contained a permanent hexahistidine tag, which could have affected the experimental observations. In this study, we purified recombinant full-length Tim44 and its C-terminal domain, which do not contain histidine tags (*23*), and examined their ability to bind sucrose-loaded liposomes in vitro. As shown in Figure 1, full-length Tim44 was able to bind cardiolipin-containing liposomes (CL/PC) with a K_d of ∼35 μM, while the affinity for cardiolipin-free vesicles (PC) was ∼7 times lower (K_d ∼ 250 μM). The presence of cardiolipin also affected the amount of protein adsorbed under saturation: the PC vesicles could bind only ∼20% of the protein measured for the CL/PC vesicles. These results essentially confirm previous observations obtained with Tim44 containing an uncleavable hexahistidine tag (*11*).

The same measurements were repeated with the purified C-terminal domain of Tim44. The results show that the purified C-terminal domain binds CL/PC and PC liposomes with similar preferences for full-length Tim44, with K_d values for the binding to CL/PC and PC liposomes of 26 and 668 μM, respectively (Figure 1). It should be mentioned that under saturation, the truncated protein had a slightly lower maximal binding capacity for the liposome, ∼60−80% with respect to that of intact Tim44 (Figures 1 and 7B).

Solution Structure of Tim44 Derived from the Simulations. In light of the results described above showing that Tim44 binds preferably to the negatively charged lipid, cardiolipin, we sought to determine whether there are specific regions of the protein that are attracted to the negatively charged headgroups of the membrane. For the sake of simplicity, we selected a fatty acid molecule, palmitate (PLM), as a model particle. Previous studies have shown that the moderate size of PLM, along with its amphipathic nature, makes it an excellent probe for detecting regions that participate in hydrophobic and/or charged interactions, over protein surfaces and inside internal cavities (*40*−*42*) We conducted unbiased MD simulations of the Tim44 C-terminal domain with charged PLM in a water box in the presence of a screening electrolyte at 100 mM. First, we simulated the C-terminal domains of human and yeast Tim44 (PDB entries 2FXT and 2CW9, respectively), in a water box containing ∼100 mM NaCl. Initial simulations were run with a system containing the protein in the electrolyte solution alone so we could evaluate the stability of the structure. Following this, extensive simulations were conducted in the presence of PLM added to the simulation box, taking care that the initial location of the PLM was more than 10 Å from the surface of the protein. The general features of the simulations are given in Table 3.

Figure 2 represents the general features of the yeast Tim44 C-terminal domain and the "elongated" C-terminal domain, as derived from a MD simulation in 100 mM NaCl. As shown in panel A, the rmsd of the proteins increased during the first 5−7 ns of the run, both for the structure as resolved by X-ray crystallography and for the elongated version. The rmsd of the crystallized structure of the protein (short Tim44) reached a level of ∼4 Å with respect to the structure at the end of the equilibration step, while that for the protein with an extension of 14 residues (elongated) was higher, up to ∼6 Å. rmsd values for the main body of the protein (inset of Figure 2A) indicate that the protein was highly stable. Apparently, most of the structural fluctuations are a reflection of helix A1 with the extension residues located at the N-terminus. When the rmsd values of three runs of the elongated structure were averaged, we found (i) for the whole protein the rmsd was 0.47 ± 0.04 nm, (ii) for helix A1 the rmsd was 0.49 ± 0.21 nm, and (iii) for the main body of the protein the rmsd was 0.24 ± 0.03 nm. From the latter values, the relative stability of the main body with respect to the N-terminus is evident.

The enhanced flexibility of the N-terminus is better illustrated in Figure 2B, where the rmsf of each residue's backbone, calculated for a 20 ns period, is plotted as a function of its

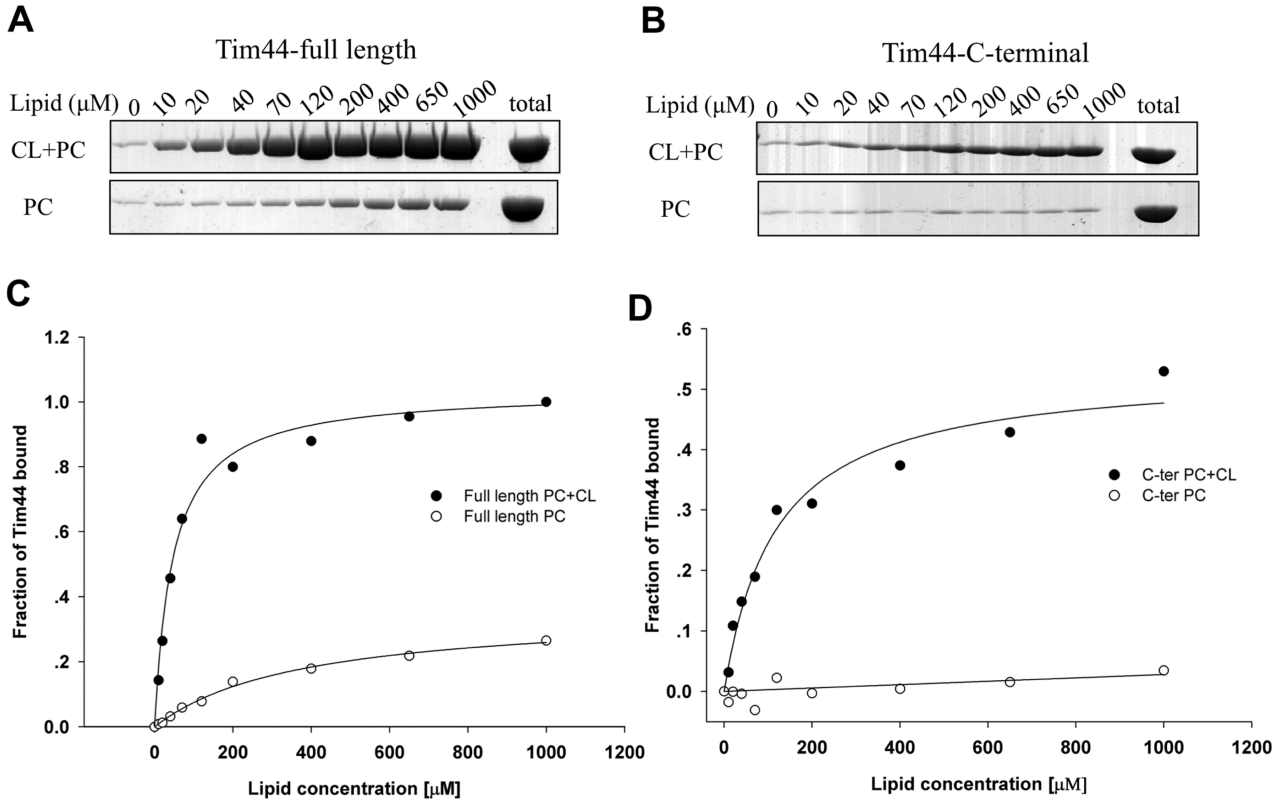

FIGURE 1: Binding of Tim44 to liposomes. One micromolar of purified full-length Tim44-full (A and C) or C-terminal domain (B and D) was incubated for 1 h with increasing concentrations of sucrose-loaded liposomes, composed of either a mixture of PC and CL (5:1) or PC alone. The liposomes were pelleted by centrifugation, and 50 μL of SDS sample buffer was added to solubilize the bound proteins. The bound fraction was analyzed by 14% SDS−PAGE and stained with Coomassie Blue. (A and B) The first 10 lanes contained increasing amounts of phospholipid. The last lane represents the total amount of added Tim44. (C and D) A quantitative representation of the binding results. The fraction of protein bound to liposomes was calculated following scanning densitometry of Coomassie-stained gels. The values are expressed as a fraction of the total amount of protein added to the experiment.

location in the protein. The black line represents the fluctuations calculated for the short Tim44 which is based on the published X-ray crystal structure. Most of the protein is rather stable, with enhanced fluctuation near the bends connecting the internally stabilized sections (α-helices and β-sheets). Toward the N-terminus, the rmsf value increases, reflecting the lack of stabilization of the "loose end". Once the N-terminus was extended by 14 additional residues (gray line), the loose end migrated to the actual N-terminus (residues 234−244), while those residues formerly fluctuating (residues 220−234) gained stability.

Altogether, the three structures exhibited the same structural features with no significant distinction among the human, yeast, and elongated yeast protein. Structural fluctuations of the protein when simulated in the presence of palmitate molecules were essentially similar to those recorded in the absence of ligand, indicating that no major structural changes took place when the ligand interacted with Tim44.

During the simulation, the PLM molecules were free to probe the aqueous phase, experiencing random encounters with the protein's surface. At 100 mM NaCl, the screening electrolyte limits the electrostatic interaction to a range of <10 Å. During the simulations, whenever the carboxylate moiety of the PLM approached 10 Å from a positive charge on the protein, the random motion of the PLM was biased and the probability of encounter with the protein was enhanced. In the same manner, the long aliphatic tail of the PLM made brief contacts with the protein as it swept through the solution. In cases where a strong Lennard-Jones interaction was formed, the motion of the PLM was arrested, enhancing the probability of a tighter encounter between the two bodies. Some of the encounters were brief, while others were more stable yet still reversible. However, in all simulations, some encounters matured into a stable complex that lasted until the simulation was terminated. A representative scenario of the protein−-PLM interaction can be found in Figure S2 of the Supporting Information.

Binding of Lipids to the Hydrophobic Pocket of Tim44. Of 11 simulations, only in one case, that for human Tim44 (Figure 3), did we observe a palmitate amphipathic molecule that was tightly associated with the hydrophobic cavity, via its hydrophobic tail, for an appreciable time, suggesting a stable encounter with Tim44. The driving force keeping the PLM in the hydrophobic cavity appears to be, exclusively, Lennard-Jones attraction, amounting to 70 ± 8 kJ/mol. The orientation of the bound lipid with its aliphatic chain inside the hydrophobic pocket and the negative carboxylate protruding into the solvent is not compatible with the identification of this pocket as the site where Tim44 associates with liposomes. The part of the bilayer that is exposed to the bulk solution, where Tim44 is located, consists of polar headgroups rather than the hydrophobic tails. Consequently, the attachment of the protein to the membrane, as in Figure 3, would require partial penetration of the protein into the membrane with major reordering of the membrane's structure. Thus, on the basis of our simulations, it is deduced that the "hydrophobic pocket" is not the primary attachment site of the protein to bilayer membranes. To further examine this possibility experimentally, we used site-directed mutagenesis to mutate

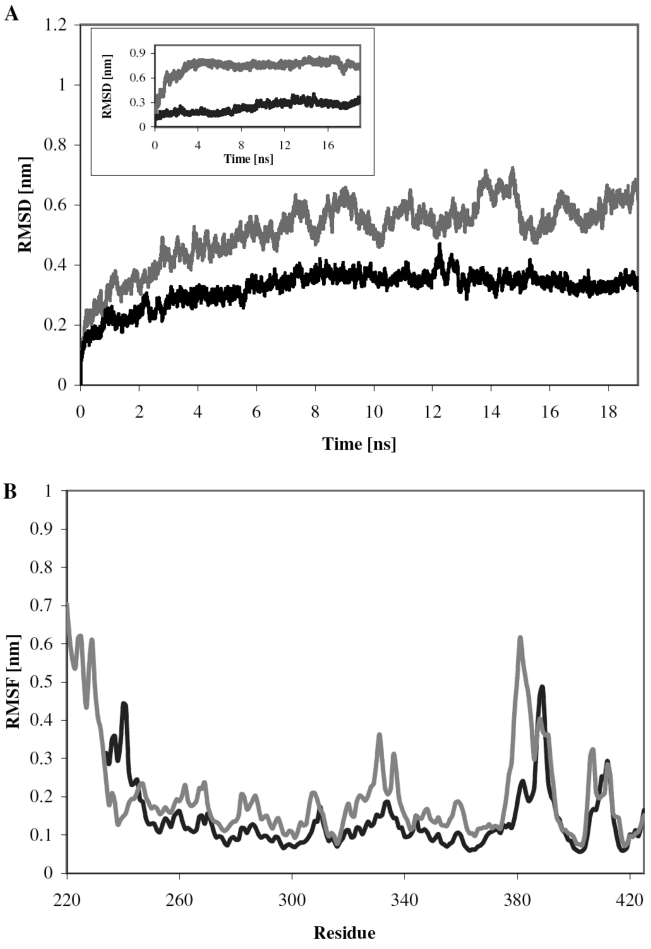

FIGURE 2: Structural stability of yeast Tim44 during molecular dynamics simulation. (A) rmsd of the Cα atoms calculated for a 20 ns simulation of the short (black line, average of 0.32 ± 0.05 nm) and elongated Tim44 (gray line, average of 0.51 ± 0.11 nm). The inset shows the rmsd of the main body of the protein (amino acids 245−425; black line, average of 0.24 ± 0.06 nm) and of the A1-elongated helix (amino acids 220−244; gray line, average of 0.74 ± 0.11 nm). (B) rms fluctuations of α-carbons of the amino acids in the short (black) and elongated protein (gray).

conserved amino acids in the hydrophobic pocket. The mutants were expressed in bacteria and subsequently purified, as described in Experimental Procedures. Unfortunately, two of the generated mutants (Y398A and F422A) were recovered in inclusion bodies. The latter result suggests that mutations of the hydrophobic cavity drastically alter the structure of the protein. However, we managed to purify two full-length Tim44 mutants, namely, V306A and G388A, that reside in the hydrophobic pocket. These two mutants demonstrated full binding to sucrose-filled liposomes, qualitatively comparable to wild-type Tim44 (Figure S3, Supporting Information).

An Alternative Lipid-Binding Site Is Observed by MD. Most of the MD simulations that were conducted with the published X-ray structures of the human and yeast Tim44 C-terminal domains ended with a PLM molecule interacting with the N-terminal section of the C-terminal domain of the protein through a combination of electrostatic and LJ attractions. To verify that the interactions are not due to the non-natural, terminal, amine moiety, α-helix A1 of the yeast protein was extended, in silico, by the addition of 14 amino acids as they appear in the sequence of the wild-type full-length protein (*22*) (for details, see Experimental Procedures).

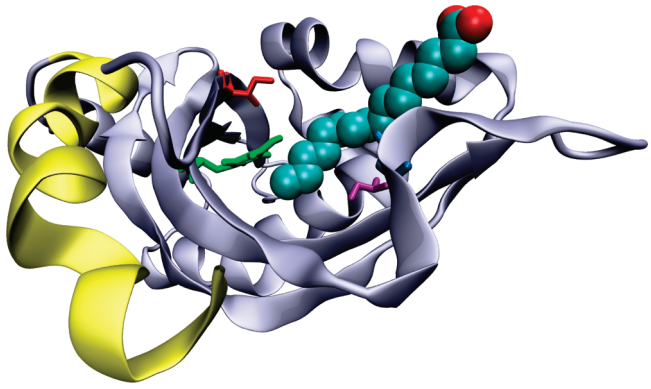

FIGURE 3: Adsorption of PLM to the hydrophobic pocket of the human Tim44 C-terminal domain. The protein is shown as a ribbon structure, while PLMs are represented by their VdW radii. A single snapshot (t = 20 ns) shows a PLM molecule located inside the hydrophobic cavity, in which the aliphatic component is interacting entirely with the protein, while the carboxylate moiety protrudes out of the pocket. Amino acids in the hydrophobic pocket that correspond to residues Y398, F422, V306, and G388 of yeast Tim44 are colored green, red, purple, and blue, respectively.

The interaction of the PLM with the protein is tracked by following the distance between the small molecule and the surface of the protein and the potential energies of the system, as exemplified in Figure 4. Panel A, which depicts the minimal distance between the two reactants, clearly demonstrates three regimes. The first one, corresponding to the first ~2 ns of the simulation time, is a random Brownian motion in which the PLM is scanning the aqueous space. The next phase of ~2−4 ns is characterized by a biased diffusion in which the distance between the two fluctuates from near contact to ~15 Å, representing the distance at which the electrostatic attraction fades because of the screening electrolyte. Within this time interval, during which the PLM is hovering near the protein, we can observe a weak electrostatic interaction between the two molecules, as represented by the rapid fluctuation of the electrostatic potential (Figure 4B). Finally, the separation between the reactants is reduced to a contact distance, and at the same time, an intensive LJ attraction is established (Figure 4B).

The LJ attraction energy appears as a time-stable potential with a magnitude of ~100 kJ/mol. In comparison, the electrostatic potential behaves in a more erratic mode, fluctuating between 0 and approximately −200 kJ/mol. The sharp fluctuations of the electrostatic potential are associated with reorientations of the carboxylate moiety with respect to local positive sites on the protein, the polar water molecules, and ions that surround it. Snapshots corresponding to the three aforementioned regimes are presented in Figure 5.

A comprehensive analysis of the contacts made between the PLM molecules and the protein is presented in Figure 6. All of the simulations were initiated with the PLM molecules located at least three water molecules from the protein surface; thus, the first phase of the simulations (≤1 ns) corresponds to the search period, before the palmitate molecules met the Tim44. Figure 6A shows plots for the encounter of PLM with Tim44 (either short or elongated) as calculated for eight independent simulations, each in the presence of four PLM molecules (Table 3). The Y axis of the plot represents the sequence of the residues of the protein, and the time vector of the simulation is given by the X axis. At any time point where the carboxylate moiety was between 3 and 4.5 Å from the protein (l), the nearest residue is marked by a blue dot.

A red dot indicates that the carboxylate was within 3 Å of the protein. Inspection of the frames reveals common qualitative features; during the first nanosecond (or sooner) of the simulation time, there were just few reversible encounters of the carboxylate with the protein (sporadic blue dots). With time, the carboxylic moiety of the PLM molecules reached attractive domains and the points of contact assume a shape of solid red lines, revealing the tendency of the PLM ions to attach themselves to preferential domains on the protein: the A1−A2 region and the sections of the structure (helices A3 and A6) that were in the proximity of the A1−A2 domain due to the folding of the unbound helices toward the rest of the protein during part of the simulations.

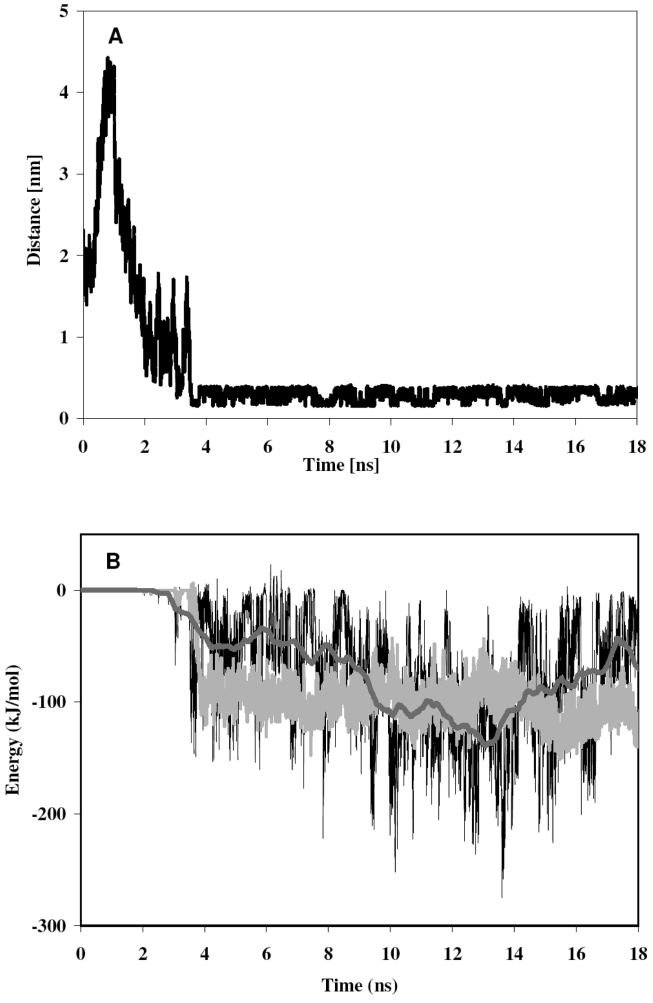

FIGURE 4: Quantitative description of the reaction between the PLM and the Tim44 protein. (A) Minimum distance of PLM from helices A1 and A2 as a function of time (in nanoseconds) (residues 220−254). (B) Energy profile of the Tim44−PLM interaction: (black line) electrostatic potential, (dark gray line) averaged electrostatic potential (every 700 ps), and (light gray line) LJ potential.

To distinguish between occasional short encounters and more significant long-lasting interactions, we display in Figure 6B the distribution of all contact events taken from all eight simulations. For this purpose, we divided the protein into three regions; helices A1 and A2 (residues 220−255), helices A3 and A6 (residues 269−282 and 318−335, respectively), and the rest of the protein. The histogram shows the accumulative contact time for a carboxylate with each of the regions. Combining the overall statistics, with the duration of contact presented in panel A, we can state that the preferred domain where the palmitate molecule adsorbs to Tim44 occurs significantly at helices A1 and A2 and the junction between them, while the rest of the protein (170 residues), having a much larger surface area than helices A1 and A2 (35 residue), hardly retains the ligand on its surface.

Comparison of the encounter density with the map of electrostatic potential (Figure 6B, inset) reveals that the binding is much more localized than the spread of the positive charges on the protein surface. Apparently, the ability of a ligand to react with a given site is a function of many interactions and cannot be identified with a single type of interaction.

It should be implicitly stated that the data presented in Figure 6 do not represent the whole "landscape of encounter" between the ligands and the protein suitable for detailed statistical thermodynamic analysis (*43*). However, there is a marked inclination of the PML molecule to prefer the A1−A2 domain of the protein. Naturally, this tendency is far from proof that this domain is the membrane binding one. To evaluate such a possibility by molecular dynamics, one may need to run the simulation for more than 1 μs (*44*). However, the involvement of the A1−A2 domain as the region of contact with the membrane has been directly confirmed by in vitro measurement, as described below.

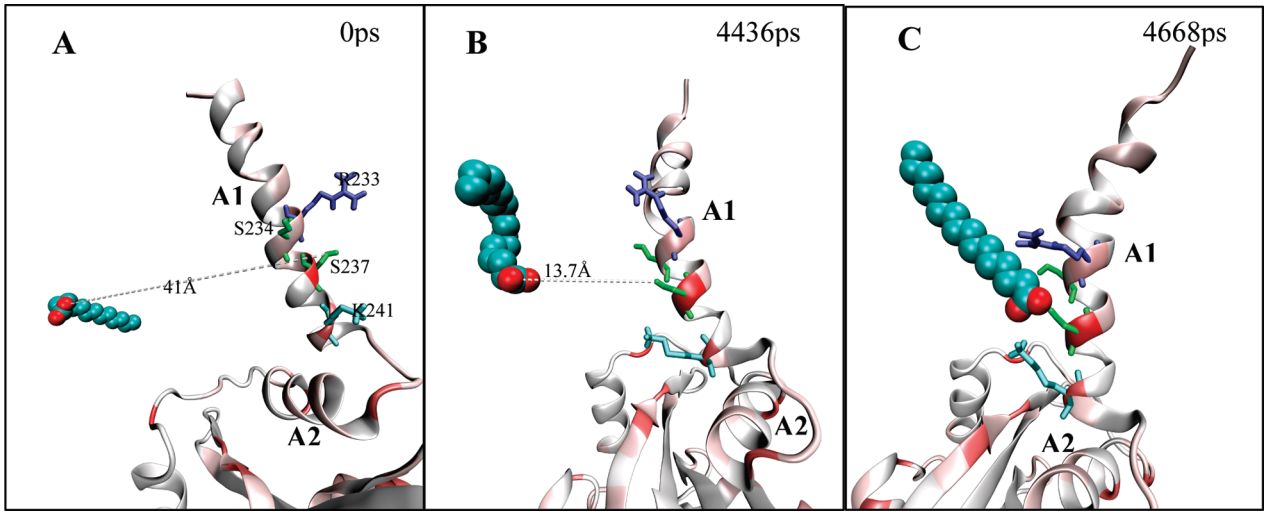

FIGURE 5: Snapshots representing the three regimes of interaction between PLM and the Tim44 protein. Panels A−C correspond to random Brownian motion, biased diffusion under electrostatic attraction, and tight binding stabilized by LJ and electrostatic potentials, respectively.

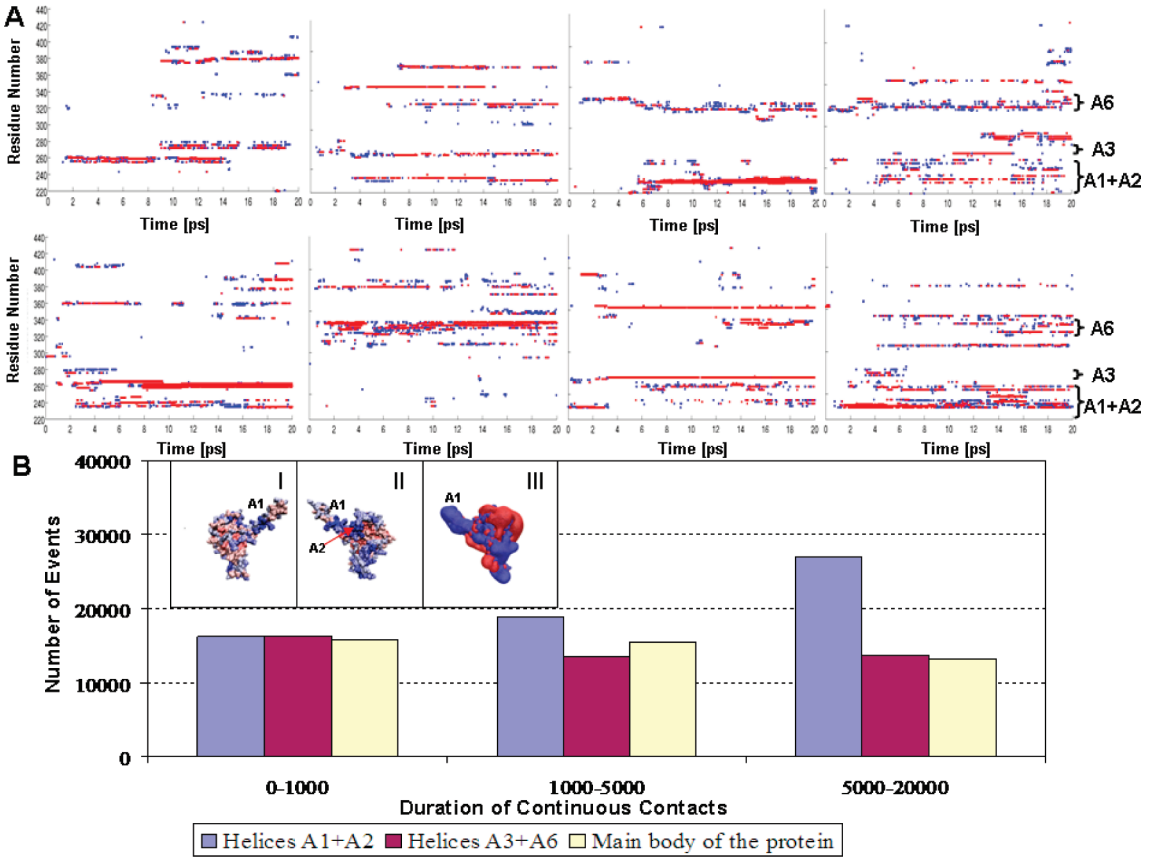

FIGURE 6: Sites of interactions of palmitate with Tim44. The figure summarizes the sites at which the carboxylate moiety of PLM was ≤4.5 Å from any residue on the protein. (A) Spatiotemporal analysis of the ligand−protein interaction of eight different simulations, as calculated for the interaction of the protein with a four-PLM molecule. The dots are for encounters between a residue (*Y* axis) and the carboxylate moiety of PLM at a given time point (*X* axis). Blue and red points imply that the distance from any carboxylate moiety to the nearest residue on the protein is 4.5−3 and <3 Å, respectively. Helices A1, A2, A3, and A6 are marked. (B) Histogram of the interactions between the carboxylate moiety of palmitate and the following specific regions of the protein: (i) helices A1 and A2 (consisting of the N-terminal section of the elongated protein), (ii) helices A3 and A6 that during the simulation time come into the proximity of helices A1 and A2, and (iii) the rest of the protein (helices A4 and A5, connecting loops, and the four core β-strands). The time length of the contacts is defined as a period during which the distance between the carboxylate and the domain is not interrupted for a time frame longer than 30 ps. Each contact event was multiplied by the number of frames it lasted. The contacts were classified as either occasional encounters lasting less than 1 ns, contacts that lasted up to 5 ns, or those that were stable for more than 5 ns. The preferred sites of interaction are presented in the inset of panel B. Boxes I and II present two views of the protein that are colored according to the propensity of the PLM molecule (any atom) to approach ($l \leq 4.5$ Å) the surface of the protein: red for zero, pink for 1−500, gray-blue for 501−1500, light blue for 1501−3000, blue for 3001−4000, and dark blue for >4000 contacts. Box III shows the electrostatic potential around the elongated C-terminal domain of Tim44, calculated by solving the Poisson−Boltzmann equation: blue envelope for a positive electric field and red for a negative electric field.

Binding of Purified N-Terminal Truncations of Tim44 to Sucrose-Loaded Vesicles. In light of the MD simulations with PLM described above, we sought confirmation for these results through in vitro binding assays. To this end, we expressed several N-terminally truncated forms of the C-terminal domain of Tim44 in bacteria, purified them, and studied their liposome binding properties in vitro. A scheme representing the various truncated forms that we prepared in this study is presented in Figure 7A. A representative binding experiment is presented in Figure 7B.

When examined for their ability to bind liposomes, the C-terminal domain and its truncations could be divided into two groups. Members of the first group bind liposomes but reached less maximal binding than full-length Tim44. As such, the C-terminal domain and the construct Tim44−235 displayed ~60−80% binding to liposomes when compared to the full-length protein. Members of the second group did not bind to liposomes. The latter group includes constructs Tim44−244 and Tim44−263. Using CD spectroscopy, we excluded the possibility that the truncations caused major changes in the structure of the protein (not shown). This is not surprising, since on the basis of the crystal structure of the C-terminal domain of yeast Tim44, the N-terminal truncations that we performed would not be expected to drastically affect the stability of the protein's C-terminal domain. It is noteworthy that two of the constructs that we examined (Tim44−244 and Tim44−263) in this study are expected to retain an intact hydrophobic pocket, based on the crystal structure of the protein (*21*, *22*). Nevertheless, the latter two constructs do not exhibit any binding to CL/PC liposomes. Altogether, the results presented above suggest that the N-terminal part of the C-terminal domain of Tim44 harbors the major membrane-binding site of this protein and that truncation of this area weakens the association of the protein with liposomes containing CL and PC.

DISCUSSION

Tim44 is a key component of the mitochondrial protein import motor. One of its important functions is to anchor components of the mitochondrial import motor (e.g., mtHsp70 and Pam/Tim proteins) to their site of action, the membranal sector of the TIM23 complex. For this purpose, Tim44 associates with the

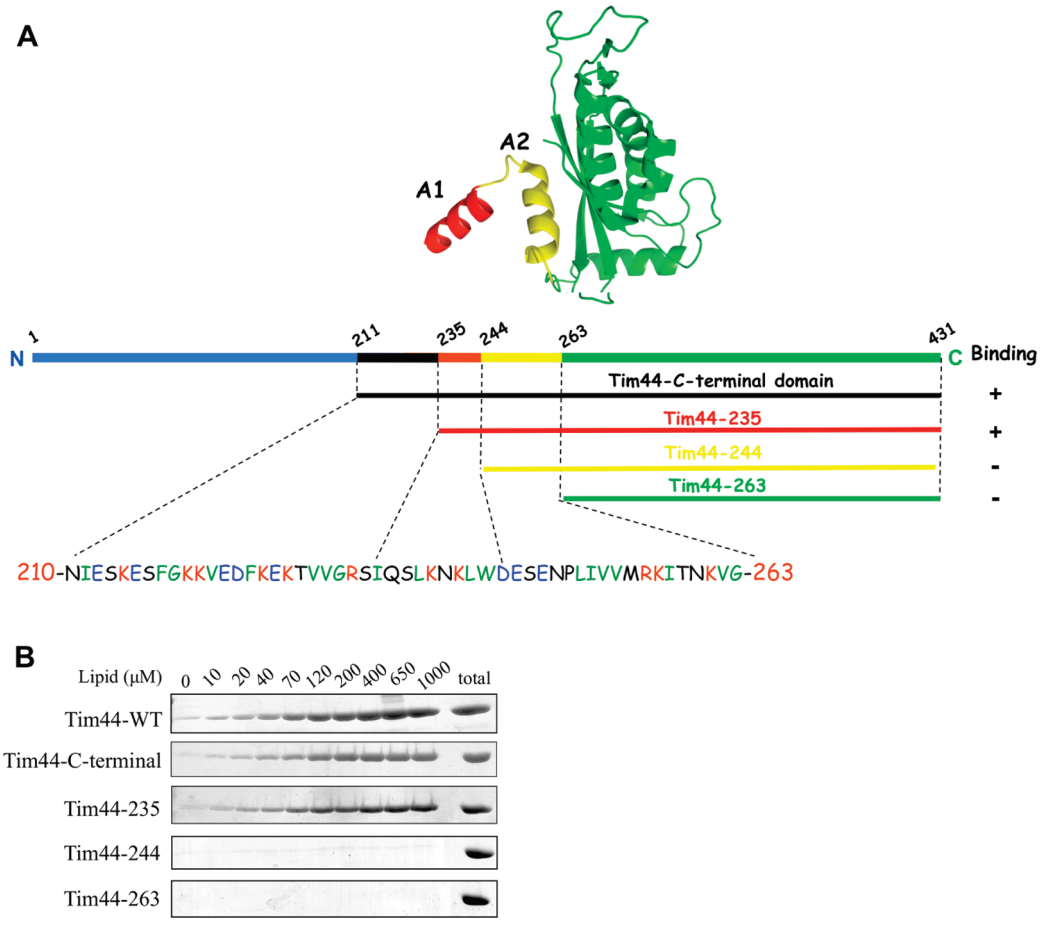

FIGURE 7: Truncated constructs of Tim44 and their ability to bind liposomes. The constructs were created according to the Tim44 C-terminal domain crystal structure [PDB entry 2FXT (*22*)]. (A) Tim44−244 (yellow arrow) and Tim44−263 (green arrow) lack helix A1 and both helices A1 and A2 of the C-terminal domain, respectively. Tim44−235 (light blue) lacks 24 amino acids. The crystal structure was determined from amino acid 234, and the C-terminal domain construct used in this work begins at amino acid 210. In the colored protein sequence, positively charged amino acids are colored red, negatively charged blue, and hydrophobic green. (B) Representative binding experiment with full-length Tim44 and its truncations to liposomes. The identity of the examined protein is indicated at the left of each gel. The experiment was conducted as described in the legend of Figure 1.

inner membrane in two ways. First, it binds the TIM23 complex directly through its association with the Tim23 protein. Second, it was shown that Tim44 associates avidly with model membranes that are enriched with the phospholipid cardiolipin (*11*). Since Tim44 is not a transmembrane protein, the latter interaction helps to keep Tim44 continuously present at its action site, the inner membrane. Recent studies indicate a very important role for cardiolipin in the biogenesis of additional mitochondrial proteins (*12*, *13*, *15*−*17*, *20*).

The major goal of this study was to identify regions of the Tim44 structure that mediate its interaction with acidic phospholipids. A previous study showed that the C-terminal domain of Tim44 retains the ability to bind acidic phospholipids (*11*). A subsequent study suggested that a hydrophobic pocket found in the structure of Tim44 serves as the lipid binding site and may explain the ability of this protein to associate with acidic phospholipids (*22*) (also reviewed in ref *45*). We used two independent methods to examine the latter hypothesis. Using the first method, MD, we showed that lipids may indeed bind within the central cavity. However, the orientation of the bound lipid (i.e., the charged head outside) cannot explain the association of Tim44 with the model membranes that do not expose hydrophobic residues toward the solution containing the protein. Indeed, when we examined the binding of two different purified, hydrophobic pocket mutants, a strong association of Tim44 with acidic phospholipids was still observed (Figure S3, Supporting Information). Unfortunately, we have not been able to examine additional double or triple mutants due to the fact that they aggregated upon expression in bacteria. MD simulations suggested an additional site that may contribute to the association of Tim44 with acidic phosholipids, namely, helices A1 and A2 at the amino-terminal side of the C-terminal domain of Tim44. The latter MD results were corroborated by the ability of purified C-terminal truncations of Tim44 to bind liposomes, in vitro. In this case, deletion of helix A1 alone abolished the ability of purified Tim44's C-terminal domain to associate with cardiolipin-containing liposomes (Figure 7A,B). It is important to note here that deletion mutants of helix A1 alone or together with A2 from the C-terminal domain of Tim44 retain their hydrophobic pockets, as can be extrapolated from the high-resolution structure of the C-terminal domain (*22*). Conversely, two constructs that contain an intact hydrophobic pocket, but not helices A1 and A2, were not able to associate with cardiolipin-containing liposomes at all (Figure 7B). The association of Tim44 with acidic phospholipids seems to require close, intimate folding of helices A1 and A2. Consequently, deletion of the former completely abolished the ability of the protein to bind liposomes. Can helices A1 and A2 confer the ability to bind cardiolipin-containing

liposomes on an unrelated protein? To answer this question, we examined the ability of a purified protein, constructed by the fusion of helices A1 and A2 to Mge1, to bind phospholipids. Two fusion constructs were examined, the first A1-A2-Mge1 carrying an amino-terminal octahisitidine tag and the second A1-A2-Mge1 in which the histidine tag was removed. Both Mge1 fusions were able to bind phospholipids containing a mixture of CL and PC (Figure 4S, Supporting Information), in a manner similar to that of full-length Tim44. However, in contrast to full-length Tim44 or its C-terminal domain, both fusions of A1-A2-Mge1 were also able to associate strongly with phospholipids composed exclusively of PC alone (Figure 4S, Supporting Information). The control Mge1$(His)_6$ did not associate with liposomes composed either of CL and PC or of PC alone (Figure 4S, Supporting Information). Thus, helices A1 and A2 confer on Mge1 the ability to associate with phospholipids in general, without retaining the specificity for liposomes containing CL. This result can be explained by the possibility that helices A1 and A2 confer the general ability to bind phospholipids and that the specificity for cardiolipin binding is granted by another, yet to be determined, region of the C-terminal domain of Tim44. Alternatively, it is possible that the cardiolipin specificity of helices A1 and A2 requires a specific folding conformation that stays intact only in the context of the folded C-terminal domain or full-length Tim44

In summary, we suggest on the basis of MD and in vitro binding assays of purified C-terminal Tim44 truncations, that helices A1 and A2 cooperate to form the major binding site of the protein for acidic phospholipids. Our results, however, do not exclude the possibility that other regions, including the hydrophobic cavity, of Tim44 may also assist in the association of Tim44 with acidic liposomes.

ACKNOWLEDGMENT

We thank Dr. Celeste Weiss-Katz for critically reading this manuscript.

SUPPORTING INFORMATION AVAILABLE

Purity of the Tim44 constructs used in this study (Figure S1), a representative scenario of the Tim44−PLM interaction (Figure S2 and a movie), binding of Tim44 mutants, on the hydrophobic cavity, to liposomes (Figure S3), and binding of A1-A2-Mge1 to liposomes (Figure S4). This material is available free of charge via the Internet at http://pubs.acs.org.

REFERENCES

1. Rapaport, D. (2005) How does the TOM complex mediate insertion of precursor proteins into the mitochondrial outer membrane? *J. Cell Biol. 171*, 419–423.
2. Mokranjac, D., and Neupert, W. (2005) Protein import into mitochondria. *Biochem. Soc. Trans. 33*, 1019–1023.
3. Pfanner, N., and Chacinska, A. (2002) The mitochondrial import machinery: Preprotein-conducting channels with binding sites for presequences. *Biochim. Biophys. Acta 1592*, 15–24.
4. Meinecke, M., Wagner, R., Kovermann, P., Guiard, B., Mick, D. U., Hutu, D. P., Voos, W., Truscott, K. N., Chacinska, A., Pfanner, N., and Rehling, P. (2006) Tim50 maintains the permeability barrier of the mitochondrial inner membrane. *Science 312*, 1523–1526.
5. Mokranjac, D., Sichting, M., Popov-Celeketic, D., Mapa, K., Gevorkyan-Airapetov, L., Zohary, K., Hell, K., Azem, A., and Neupert, W. (2009) Role of Tim50 in the transfer of precursor proteins from the outer to the inner membrane of mitochondria. *Mol. Biol. Cell 20*, 1400–1407.
6. Stojanovski, D., Rissler, M., Pfanner, N., and Meisinger, C. (2006) Mitochondrial morphology and protein import-A tight connection? *Biochim. Biophys. Acta 1763*, 414–421.
7. Popov-Celeketic, D., Mapa, K., Neupert, W., and Mokranjac, D. (2008) Active remodelling of the TIM23 complex during translocation of preproteins into mitochondria. *EMBO J. 27*, 1469–1480.
8. Chacinska, A., Lind, M., Frazier, A. E., Dudek, J., Meisinger, C., Geissler, A., Sickmann, A., Meyer, H. E., Truscott, K. N., Guiard, B., Pfanner, N., and Rehling, P. (2005) Mitochondrial presequence translocase: Switching between TOM tethering and motor recruitment involves Tim21 and Tim17. *Cell 120*, 817–829.
9. Mokranjac, D., Popov-Celeketic, D., Hell, K., and Neupert, W. (2005) Role of Tim21 in mitochondrial translocation contact sites. *J. Biol. Chem. 280*, 23437–23440.
10. van der Laan, M., Chacinska, A., Lind, M., Perschil, I., Sickmann, A., Meyer, H. E., Guiard, B., Meisinger, C., Pfanner, N., and Rehling, P. (2005) Pam17 is required for architecture and translocation activity of the mitochondrial protein import motor. *Mol. Cell. Biol. 25*, 7449–7458.
11. Weiss, C., Oppliger, W., Vergeres, G., Demel, R., Jeno, P., Horst, M., de Kruijff, B., Schatz, G., and Azem, A. (1999) Domain structure and lipid interaction of recombinant yeast Tim44. *Proc. Natl. Acad. Sci. U. S.A. 96*, 8890–8894.
12. Osman, C., Haag, M., Potting, C., Rodenfels, J., Dip, P. V., Wieland, F. T., Brugger, B., Westermann, B., and Langer, T. (2009) The genetic interactome of prohibitins: Coordinated control of cardiolipin and phosphatidylethanolamine by conserved regulators in mitochondria. *J. Cell Biol. 184*, 583–596.
13. Kutik, S., Rissler, M., Guan, X. L., Guiard, B., Shui, G., Gebert, N., Heacock, P. N., Rehling, P., Dowhan, W., Wenk, M. R., Pfanner, N., and Wiedemann, N. (2008) The translocator maintenance protein Tam41 is required for mitochondrial cardiolipin biosynthesis. *J. Cell Biol. 183*, 1213–1221.
14. Haines, T. H., and Dencher, N. A. (2002) Cardiolipin: A proton trap for oxidative phosphorylation. *FEBS Lett. 528*, 35–39.
15. Liu, Z., Ho, L., and Bonning, B. (2007) Localization of a *Drosophila melanogaster* homolog of the putative juvenile hormone esterase binding protein of *Manduca sexta*. *Insect Biochem. Mol. Biol. 37*, 155–163.
16. Ott, M., Zhivotovsky, B., and Orrenius, S. (2007) Role of cardiolipin in cytochrome c release from mitochondria. *Cell Death Differ. 14*, 1243–1247.
17. Claypool, S. M. (2009) Cardiolipin, a critical determinant of mitochondrial carrier protein assembly and function. *Biochim. Biophys. Acta 1788*, 2059–2068.
18. Schlattner, U., Gehring, F., Vernoux, N., Tokarska-Schlattner, M., Neumann, D., Marcillat, O., Vial, C., and Wallimann, T. (2004) C-Terminal lysines determine phospholipid interaction of sarcomeric mitochondrial creatine kinase. *J. Biol. Chem. 279*, 24334–24342.
19. van der Laan, M., Meinecke, M., Dudek, J., Hutu, D. P., Lind, M., Perschil, I., Guiard, B., Wagner, R., Pfanner, N., and Rehling, P. (2007) Motor-free mitochondrial presequence translocase drives membrane integration of preproteins. *Nat. Cell Biol. 9*, 1152–1159.
20. Lionaki, E., de Marcos Lousa, C., Baud, C., Vougioukalaki, M., Panayotou, G., and Tokatlidis, K. (2008) The essential function of Tim12 in vivo is ensured by the assembly interactions of its C-terminal domain. *J. Biol. Chem. 283*, 15747–15753.
21. Handa, N., Kishishita, S., Morita, S., Akasaka, R., Jin, Z., Chrzas, J., Chen, L., Liu, Z. J., Wang, B. C., Sugano, S., Tanaka, A., Terada, T., Shirouzu, M., and Yokoyama, S. (2007) Structure of the human Tim44 C-terminal domain in complex with pentaethylene glycol: Ligand-bound form. *Acta Crystallogr. D63*, 1225–1234.
22. Josyula, R., Jin, Z., Fu, Z., and Sha, B. (2006) Crystal structure of yeast mitochondrial peripheral membrane protein Tim44p C-terminal domain. *J. Mol. Biol. 359*, 798–804.
23. Slutsky-Leiderman, O., Marom, M., Iosefson, O., Levy, R., Maoz, S., and Azem, A. (2007) The interplay between components of the mitochondrial protein translocation motor studied using purified components. *J. Biol. Chem. 282*, 33935–33942.
24. Azem, A., Oppliger, W., Lustig, A., Jeno, P., Feifel, B., Schatz, G., and Horst, M. (1997) The mitochondrial hsp70 chaperone system. Effect of adenine nucleotides, peptide substrate, and mGrpE on the oligomeric state of mhsp70. *J. Biol. Chem. 272*, 20901–20906.
25. Buser, C. A., and McLaughlin, S. (1998) Ultracentrifugation technique for measuring the binding of peptides and proteins to sucrose-loaded phospholipid vesicles. *Methods Mol. Biol. 84*, 267–281.
26. Vergeres, G., Manenti, S., Weber, T., and Sturzinger, C. (1995) The myristoyl moiety of myristoylated alanine-rich C kinase substrate (MARCKS) and MARCKS-related protein is embedded in the membrane. *J. Biol. Chem. 270*, 19879–19887.
27. Berendsen, H. J. C., van der Spoel, D., and van Drunen, R. (1995) GROMACS: A message-passing parallel molecular dynamics implementation. *Comput. Phys. Commun. 91*, 43–56.

28. Lindahl, E., Hess, B., and van der Spoel, D. (2001) Gromacs 3.0: A package for molecular simulation and trajectory analysis. *J. Mol. Model. 7*, 306–317.
29. Van der Spoel, D., Lindahl, E., Hess, B., Groenhof, G., Mark, A. E., and Berendsen, H. J. C. (2005) GROMACS: Fast, flexible, and free. *J. Comput. Chem. 26*, 1701–1718.
30. Oostenbrink, C., Villa, A., Mark, A. E., and Van Gunsteren, W. F. (2004) A biomolecular force field based on the free enthalpy of hydration and solvation: The GROMOS force-field parameter sets 53A5 and 53A6. *J. Comput. Chem. 25*, 1656–1676.
31. Berman, H. M., Westbrook, J., Feng, Z., Gilliland, G., Bhat, T. N., Weissig, H., Shindyalov, I. N., and Bourne, P. E. (2000) The Protein Data Bank. *Nucleic Acids Res. 28*, 235–242.
32. Guex, N., and Peitsch, M. C. (1997) SWISS-MODEL and the Swiss-PdbViewer: An environment for comparative protein modeling. *Electrophoresis 18*, 2714–2723.
33. Schuttelkopf, A. W., and van Aalten, D. M. (2004) PRODRG: A tool for high-throughput crystallography of protein-ligand complexes. *Acta Crystallogr. D60*, 1355–1363.
34. Berendsen, H. J. C., Postma, J. P. M., van Gunsteren, W. F., and Hermans, J. (1969) Interaction Models for Water in Relation to Protein Hydration. *Nature 224*, 175–177.
35. Hess, B., Bekker, H., Berendsen, H. J. C., and Fraaije, J. G. E. M. (1997) LINCS: A linear constraint solver for molecular simulations. *J. Comput. Chem. 18*, 1463–1472.
36. Miyamoto, S., and Kollman, P. A. (1992) SETTLE: An Analytical Version of the SHAKE and RATTLE Algorithms for Rigid water models. *J. Comput. Chem. 13*, 952–962.
37. Berendsen, H. J. C., Postma, J. P. M., DiNola, A., and Haak, J. R. (1984) Molecular dynamics with coupling to an external bath. *J. Chem. Phys. 81*, 3684–3690.
38. Essman, U., Perela, L., Berkowitz, M. L., Darden, T., Lee, H., and Pederse, L. G. (1995) A smooth particle mesh Ewald method. *J. Chem. Phys. 103*, 8577–8592.
39. Humphrey, W., Dalke, A., and Schulten, K. (1996) VMD: Visual molecular dynamics. *J. Mol. Graphics 14*, 33–38.
40. Friedman, R., Nachliel, E., and Gutman, M. (2005) Molecular Dynamics Simulations of the Adipocyte Lipid Binding Protein Reveal a Novel Entry Site for the Ligand. *Biochemistry 44*, 4275–4283.
41. Tsfadia, Y., Friedman, R., Kadmon, J., Selzer, A., Nachliel, E., and Gutman, M. (2007) Molecular dynamics simulations of palmitate entry into the hydrophobic pocket of the fatty acid binding protein. *FEBS Lett. 581*, 1243–1247.
42. Levin, L. B., Nachliel, E., Gutman, M., and Tsfadia, Y. (2009) Molecular dynamics study of the interaction between fatty acid binding proteins with palmitate mini-micelles. *Mol. Cell. Biochem. 326*, 29–33.
43. Grossfield, A., Feller, S. E., and Pitman, M. C. (2007) Convergence of molecular dynamics simulations of membrane proteins. *Proteins 67*, 31–40.
44. Khelashvili, G., Grossfield, A., Feller, S. E., Pitman, M. C., and Weinstein, H. (2009) Structural and dynamic effects of cholesterol at preferred sites of interaction with rhodopsin identified from micro-second length molecular dynamics simulations. *Proteins 76*, 403–417.
45. Mokranjac, D., and Neupert, W. (2009) Thirty years of protein translocation into mitochondria: Unexpectedly complex and still puzzling. *Biochim. Biophys. Acta 1793*, 33–41.